2020-01-0999 Published 14 Apr 2020

Integrated Model Predictive Control and Adaptive Unscented Kalman Filter for Semi-Active Suspension System Based on Road Classification

Zhenfeng Wang, Shengjie Xu, Fei Li, Xinyu Wang, and Jiansen Yang
China Automotive Technology and Research Center Co., Ltd.

Jing Miao Suzhou University of Science and Technology

Citation: Wang, Z., Xu, S., Li, F., Wang, X. et al., "Integrated Model Predictive Control and Adaptive Unscented Kalman Filter for Semi-Active Suspension System Based on Road Classification," SAE Technical Paper 2020-01-0999, 2020, doi:10.4271/2020-01-0999.

Abstract

The accuracy of state estimation and optimal control for controllable suspension system is a challenging task for the vehicle suspension system under various road excitations. How to effectively acquire suspension states and choose the reasonable control algorithm become a hot topic in both academia and industry. Uncertainty is unavoidable for the suspension system, e.g., varying sprung or unsprung mass, suspension damping force or spring stiffness. To tackle the above problems, a novel observer-based control approach, which combines adaptive unscented Kalman filter (AUKF) observer and model predictive control (MPC), is proposed in the paper. A quarter semi-active suspension nonlinear model and road profile model are first established. Secondly, using the road classification identification method based on system response, an AUKF algorithm is employed to estimate accurately the state of suspension system. Due to the nonlinear of semi-active suspension damping force in the movement process, the methods of observer-based and model predictive control are used to design the optimal predictive controller under various road excitations. Finally, compared with passive suspension system, the constrained optimal control (COC) algorithm and the model predictive control (MPC) algorithm, the road handing and ride comfort indexes are analyzed. Simulation results show that the performance of the proposed model predictive control algorithm compared with passive mode for the semi-suspension system improves more than 10% under the same road excitation condition.

1. Introduction

Controllable suspension systems play a core role in modern vehicle technologies, particularly to improve vehicle chassis performance. Therefore, it is imperative that the state inputs for controllable suspension systems are accurate [1, 2]. Due to cost-savings and high accuracy, state observers are widely used in controllable suspension system processes [3]. Many methods have been adopted to precisely acquire the state of a suspension system, and the most known algorithm is the Kalman Filter (KF), which is used to estimate inaccurate and unmeasurable system inputs [4]. However, the KF requires some key assumptions, such as that the system model should be exact, and the statistical characteristics of the process noise and measurement noise must be white Gaussian. Real-world suspension systems have considerable nonlinearities due to time-varying parameters and road excitations. Hence, high-accuracy state observers may not be achieved using the traditional KF. To deal with the above mentioned, extended Kalman filter (EKF) [5, 6] and Unscented Kalman Filter (UKF) are proposed to improve the accuracy of nonlinear filtering [7, 8]. In [5], EKF is used to estimate the road grade in current situation. Results show that the proposed EKF algorithm can be obtained higher accuracy and faster convergence speed, compared with the traditional KF. In [7], the proposed adaptive UKF (AUKF) is used to estimate vehicle system movement state. Simulation results show that the proposed approach has higher accuracy for system state estimation under different international organization for standardization (ISO) road input conditions. In [9], a dual UKF is designed to identify parameters and state for vehicle system. The proposed approach is validated by using the simulation and experimental results. Furthermore, a UKF algorithm is widely applied to calculate higher accurate suspension system movement state.

Uncertain disturbance may induce significant degradation in observer or control quality of system estimations. When disturbance suddenly occurred, the system error of state observer and control algorithm become significant. The performance of model-based control algorithms may led to instability in this condition [3, 10]. Based on the aforementioned discussion, many observer-based control algorithm are designed to improve the performance of researching system, such as robust control, sliding mode control, model

predictive control and so on. In [11], a new multivariable linear parameter varying (LPV) H∞ control algorithm is proposed to handle critical driving situations for global vehicle chassis system. Compared with the traditional LPV algorithm, simulation results show that the proposed method is validated using the same simulation scenarios. In [12], the conception of Vehicle-to-Cloud-to-Vehicle (V2C2V) is used to develop a novel framework of simultaneous vehicle estimation and anomaly detection by combing a jump diffusion process algorithm and a multi-input observer. The real vehicle test and simulation results show that the proposed approach is effective. In [13], combining with model predictive control (MPC) algorithm, a new damper with four discrete damping modes is applied to vehicle semi-active air suspension. Simulation results show that the efficacy of the proposed approach control is validated. In [14], the Takagi-Sugeno (T-S) fuzzy control algorithm is developed to deal with the adaptive sliding mode control algorithm for active suspension system. Simulations results indicate that the effectiveness of the proposed approach is proved using the half-vehicle active suspension model. However, all of the mentioned studied do not fully consider for improving performance of controllable suspension system under the various road excitations.

To tackle the above-mentioned questions, the following contributions are considered in this paper:

- The AUKF algorithm based road classification is formed to estimate the couple state of semi-active suspension system under the various road excitations.
- The observer-based MPC algorithm is designed to improve the performance of road handing and ride comfort. Compared with the other methods, the proposed algorithm is validated and the accuracy of improving performance is more than 10%.

In this paper, a novel observer-based MPC algorithm for efficient performance improving based on AUKF observer is proposed. More details with the approach state as follows. System modeling with a quarter semi-active suspension and road excitation are firstly established. Secondly, based on the road classification method, an AUKF algorithm is proposed to estimate the couple state of suspension system. Then, the observer-based MPC algorithm is developed to improve the performance of vehicle chassis. Finally, compared with the passive suspension and constrained optimal control (COC) algorithm, the proposed approach is validated under the same road excitations.

The rest of this paper is organized as follows. Road excitation and suspension system models are briefly reviewed in Section 2. In Section 3, an AUKF algorithm is proposed based road classification, before the joint model-based AUKF and MPC algorithm is produced in Section 4. Section 5 shows simulation results of the proposed algorithm for the suspension system performance application and a comparison of its control effectiveness with other optimal control algorithm under the same driving conditions. Finally, the conclusions are given in Section 6.

2. Road Profile and Suspension System Model

2.1. Road Profile Modelling

A two dimension (2-D) road roughness parameter can be defined based the Fourier transform and the power spectral density (PSD) of 1-D road profile [15] as:

$$G_q(n) = G_q(n_0)\left(\frac{n}{n_0}\right)^{-w} \tag{1}$$

Where, n represents the spatial frequency (m^{-1}), n_0 is the reference spatial frequency (0.1 m^{-1}), $G_q(n_0)$ represents the PSD value (m^3) and w represents the termed waviness, which is commonly taken as w=2. $G_q(n_0)$ are the different road levels from ISO-*A* to ISO-*H*.

The frequent problem of road estimation errors at low frequencies is overcome by developing a method for road production based on a rational white noise signal [16], and thus the PSD of the road profile can be calculated as:

$$G_q(n) = \frac{\varepsilon\eta^2}{\pi\left(\varepsilon^2 + n^2\right)} \tag{2}$$

Where, ε represents a constant related to the road features and η^2 is a variable for the road roughness.

Considering the time domain representation and white noise covariance, the corresponding equation can be calculated as follows:

$$\mathrm{cov}\left[w(t)\right] = E\left[w(t)w(t+\tau)\right] = 2\rho^2\varepsilon v\delta(\tau) \tag{3}$$

Where, $w(t)$ is the white noise sequence; v is the velocity of the vehicle (m/s); τ is the time-shift (s) and $\delta(\tau)$ is the impulse function. Based on the nonlinear identification method of Least Squares observer, identifiable parameters for Eq. (2) are listed in Table 1. More details can be found in [17, 18].

Using the value mentioned above, the PSD can be calculated using the proposed method, and the results are shown in Figure 1. Figure 1 shows consistent results for the PSD of the road profile produced using rational white noise and the ISO standard.

TABLE 1 Identified parameters of the road profile

Road Level	$\varepsilon/(m^{-1})$	η/m	$G_q(n_0)$
ISO-*A*	0.0011	0.0153	16
ISO-*B*	0.0011	0.0306	64
ISO-*C*	0.0011	0.0611	256
ISO-*D*	0.0011	0.1222	1024
ISO-*E*	0.0011	0.2444	4096
ISO-*F*	0.0011	0.4888	16384
ISO-*G*	0.0011	0.9776	65536
ISO-*H*	0.0011	1.9552	262144

FIGURE 1 Results of estimated parameters

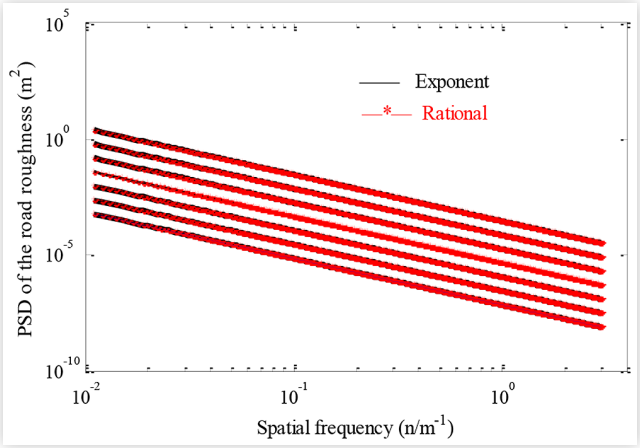

2.2. Suspension System Modelling

In this section, a commonly-used nonlinear model for vehicle suspension system is presented, and the structure of a semi-active Macpherson suspension is shown in Figure 2(a). Due to the special analysis of nonlinear suspension systems, we can ignore the mass of the arm and assume it to be a pin joint for the bushing. Then, the simple semi-active Macpherson suspension is illustrated in Figure 2(b) [16].

A two degree of freedom (2DOF) model is obtained using a method from previous studies [19], and the semi-active Macpherson suspension nonlinear model can be obtained as follows:

$$
\begin{aligned}
&m_w l_{oc}^{\,2}\ddot{\theta} + m_w l_{oc}\cos(\theta+\theta_0)\ddot{x}_b + \frac{1}{2}k_s b_l \sin(\alpha'-\theta) \\
&+ \frac{k_s[(-a_l b_l)\sin(\alpha'-\theta) + b_l^2\sin(\alpha'-\theta)\cos\alpha']}{2\sqrt{a_l^2 - a_l b_l[\cos(\alpha'-\theta)+\cos\alpha'] + b_l^2\cos\alpha'\cos(\alpha'-\theta)}} \\
&+ k_t\left\{x_b + l_{oc}\left[\sin(\theta+\theta_0) - \sin\theta_0\right] - x_r\right\} l_{oc}\cos(\theta+\theta_0) \\
&+ \frac{c b_l^2 \dot{\theta}\sin^2(\alpha'-\theta)}{4\left[a_l - b_l\cos(\alpha'-\theta)\right]} = 0
\end{aligned}
\tag{4}
$$

$$
\begin{aligned}
&m_b\ddot{x}_b + m_w l_{oc}\ddot{\theta}\cos(\theta+\theta_0) - m_w l_{oc}\sin(\theta+\theta_0)\dot{\theta}^2 \\
&-\left(\frac{1}{2}k_s b_l \sin(\alpha'-\theta)\right) - \frac{c b_l^2\dot{\theta}}{4\left[a_l - b_l\cos(\alpha'-\theta)\right]} \\
&+ k_t\left\{x_b + l_{oc}\left[\sin(\theta+\theta_0) - \sin\theta_0\right] - x_r\right\} = 0
\end{aligned}
\tag{5}
$$

Where, k_s and k_t are the suspension and tire spring stiffness, respectively; c is the damping of the suspension, x_b and $\ddot{x}_b$ represent the displacement and acceleration of the sprung mass; x_r represents the road profile, and θ_0, θ and $\dot{\theta}$ represent the initial angular, normal angular, and angular velocity of the suspension arm respectively. l_{oc}, l_{ob} and l_{oa} represent the distances between point O and point C, and B and A, respectively, and $\alpha' = \alpha + \theta_0$, $a_l = l^2_{OA} + l^2_{OB}$, $b_l = 2l_{OA}l_{OB}$.

FIGURE 2 Semi-active Macpherson suspension system; (a) Structure of the system, (b) Simplified system

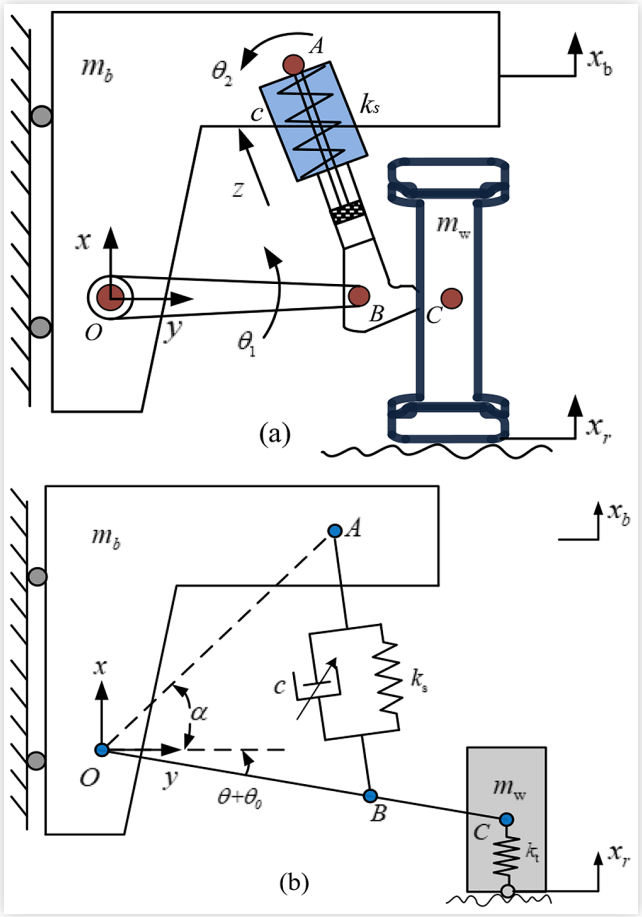

To further illustrate the nonlinear relationship between various components of the suspension system, the linearization model state can be obtained as follows.

Firstly, the state parameters are defined as $[x_1, x_2, x_3, x_4]$ $T = [x_b, \dot{x}_b, \theta, \dot{\theta}]T$.

$$
\begin{aligned}
\dot{x}_1 &= x_2, \qquad \dot{x}_2 = f_1(x_1, x_2, x_3, x_4, x_r) \\
\dot{x}_3 &= x_4, \qquad \dot{x}_4 = f_2(x_1, x_2, x_3, x_4, x_r)
\end{aligned}
\tag{6}
$$

And,

$$
f_1 = \frac{1}{D_1}\left\{\begin{matrix} m_w l_{oc}\sin(x_3+\theta_0)x_4^2 - \frac{1}{2}k_s\sin(\alpha'-x_3)\cos(x_3-\theta_0)g(x_3) \\ +ch(x_3)\dot{\theta} - k_t l_{OC}\sin^2(x_3-\theta_0)z(\cdot) \end{matrix}\right\}
$$

$$
f_2 = \frac{1}{D_2}\left\{\begin{matrix} m^2{}_w l^2{}_{OC}\sin(x_3-\theta_0)\cos(x_3-\theta_0)x_4^2 + (m_b+m_w)ch(x_3)x_4 \\ -\frac{1}{2}k_s(m_b+m_w)\sin(\alpha'-x_3)\cos(x_3-\theta_0)g(x_3) \\ +m_b k_t l_{OC}\cos(x_3-\theta_0)z(\cdot) \end{matrix}\right\}
$$

$$D_1 = m_b l_{OC} + m_w l_{OC} sin^2\left(x_3 - \theta_0\right);$$

$$D_2 = m_b m_w l^2{}_{OC} + m^2{}_w l^2{}_{OC} sin^2\left(x_3 - \theta_0\right);$$

$$h\left(x_3\right) = \frac{b_l^2 sin^2\left(\alpha' - x_3\right)}{4\left(a_l - b_l cos\left(\alpha' - x_3\right)\right)};$$

$$z(\cdot) = z\left(x_1, x_2, x_r\right) = x_1 + l_{OC}\left(sin\left(x_3 - \theta_0\right) + sin\left(\theta_0\right)\right) - x_r$$

$$g(x_3) = b_l + \frac{a_l b_l - b_l^2 cos(\alpha + \theta_0)}{\sqrt{(a_l^2 - a_l b_l cos(\alpha + \theta_0) - a_l b_l - b_l^2 cos(\alpha + \theta_0) cos(\alpha' - x_3))}}$$

The corresponding linear state equation is then expressed as follows. Further details can be found in [20].

$$\dot{x}_1 = Ax\left(t\right) + Bx_r\left(t\right), \qquad x\left(0\right) = x_0 \tag{7}$$

And,

$$A = \begin{bmatrix} 0 & 1 & 0 & 0 \\ \frac{\partial f_1}{\partial x_1} & \frac{\partial f_1}{\partial x_2} & \frac{\partial f_1}{\partial x_3} & \frac{\partial f_1}{\partial x_4} \\ 0 & 0 & 0 & 1 \\ \frac{\partial f_2}{\partial x_1} & \frac{\partial f_2}{\partial x_2} & \frac{\partial f_2}{\partial x_3} & \frac{\partial f_2}{\partial x_4} \end{bmatrix}_{x_e}; \quad B = \begin{bmatrix} 0 & \frac{\partial f_1}{\partial z_r} & 0 & \frac{\partial f_2}{\partial z_r} \end{bmatrix}_{z_r = 0}$$

Based on the above analysis, a linear suspension model is established that includes basic vertical movement information [21, 22]. The structure of the linear suspension system is shown in Figure 3.

The dynamic equations of the semi-active suspension system are given as:

$$\begin{aligned} m_b \ddot{x}_b + k_s\left(x_b - x_w\right) + u = 0 \\ m_w \ddot{x}_w + k_t\left(x_w - x_r\right) + k_s\left(x_w - x_b\right) - u = 0 \end{aligned} \tag{8}$$

Where, u is the semi-active suspension damping force. k_t and k_s are the tire spring stiffness and the suspension stiffness, respectively. x_b, $\dot{x}_b$ and $\ddot{x}_b$ represent the displacement, velocity and acceleration of the sprung mass, respectively and x_w, $\dot{x}_w$ and $\ddot{x}_w$ represent the displacement, velocity and acceleration of the unsprung mass, respectively. x_r represents the road roughness.

The corresponding system state and measure vectors are given by:

$$\mathbf{x} = \left[x_b - x_w, x_w - x_r, \dot{x}_b, \dot{x}_w\right]^T; \quad \mathbf{y} = \left[\ddot{x}_b, \ddot{x}_w\right]^T$$

Where, the four states represent the rattle space, tire deflection, velocity of the sprung mass and the velocity of unsprung mass, respectively and the two output states are the acceleration of the sprung mass and the unsprung mass, respectively.

The state space variables of the semi-active suspension system can then be obtained as:

$$\begin{aligned} \dot{\mathrm{x}} = \mathrm{Hx} + \mathrm{F}\hat{u} + \Gamma w \\ \mathrm{y} = \mathrm{Cx} + \mathrm{D}\hat{u} + \mathrm{v} \end{aligned} \tag{9}$$

FIGURE 3 Model of semi-active suspension system

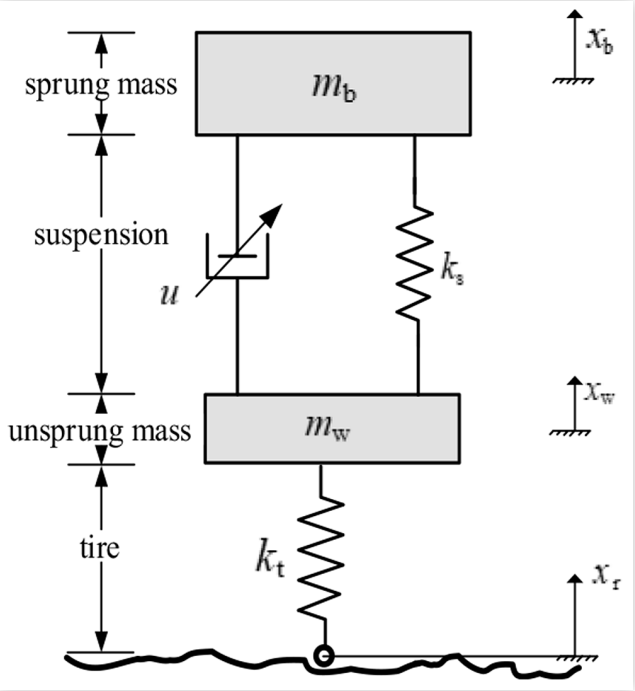

And,

$$H = \begin{bmatrix} 0 & 0 & 1 & -1 \\ 0 & 0 & 0 & 1 \\ -\frac{k_s}{m_b} & 0 & 0 & 0 \\ \frac{k_s}{m_w} & -\frac{k_t}{m_w} & 0 & 0 \end{bmatrix}, \quad F = \begin{bmatrix} 0 \\ 0 \\ -\frac{1}{m_b} \\ \frac{1}{m_w} \end{bmatrix}, \quad \Gamma = \begin{bmatrix} 0 \\ -1 \\ 0 \\ 0 \end{bmatrix},$$

$$C = \begin{bmatrix} -\frac{k_s}{m_b} & 0 & 0 & 0 \\ \frac{k_s}{m_w} & -\frac{k_t}{m_w} & 0 & 0 \end{bmatrix}, \quad D = \begin{bmatrix} -\frac{1}{m_b} \\ \frac{1}{m_w} \end{bmatrix};$$

$$\hat{u} = c \cdot \left(\dot{x}_b - \dot{x}_w\right); \quad w = \dot{x}_r;$$

Where, c is the controllable suspension system damping, w is the process noise and v is the measurement noise. All variables are assumed to be independent and Gaussian. $\dot{x}_r$ is the velocity of the road roughness and the equivalent discrete-time formula corresponding to Eq. (4) and Eq. (5) can be found in [23, 24, 25].

Based on the above mentioned, the corresponding estimated parameters of semi-active suspension are listed in Table 2.

To further validate the effective of the linearization model for semi-active suspension, we assume that the parameters of system damping are firstly chosen as 2000Ns/m. Using Table 2 section parameters, the responses of the displacement of rattle space and tire; the acceleration of sprung mass and unsprung mass are compared various models under ISO road excitation.

TABLE 2 Values of *Q* and *R* of suspension system under various road input

System Parameters	Symbol & Unit	Value
Sprung mass	m_b (kg)	410
Unsprung mass	m_w (kg)	40
Suspension spring stiffness	k_s (N/m)	20000
Tire stiffness	k_t (N/m)	183000
Maximum damping	c_{max} (Ns/m)	2500
Minimum damping	c_{min} (Ns/m)	600

FIGURE 4 Results of various models with response state under ISO-*E* road input

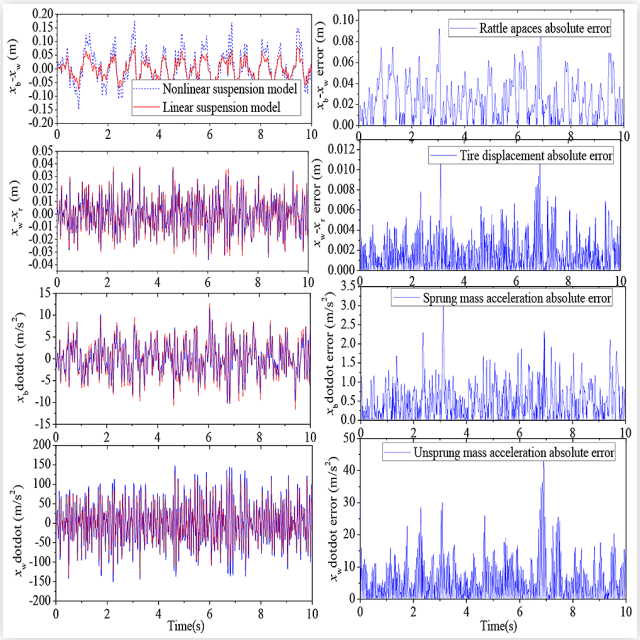

Results with system response and absolute error for various models based on ISO-*E* input are shown in Figure 4.

Figure 4 illustrates that the responses absolute error value of various models are acceptable under ISO-*E* road excitation. Then, the linear suspension model can be used as follows.

3. Analysis for AUKF Algorithm Based Road Classification

3.1. Representation for Road Classification Approach

In this section, the structure of the proposed road classifier based on the system responses is shown in Figure 5 [26]. Figure 5 shows the process of the proposed approach, and more details can be explained as followed.

Step 1: Signals Sampling & Pre-processing. The acceleration of sprung mass and unsprung mass, rattle space of

FIGURE 5 Flaw chart of road classification approach

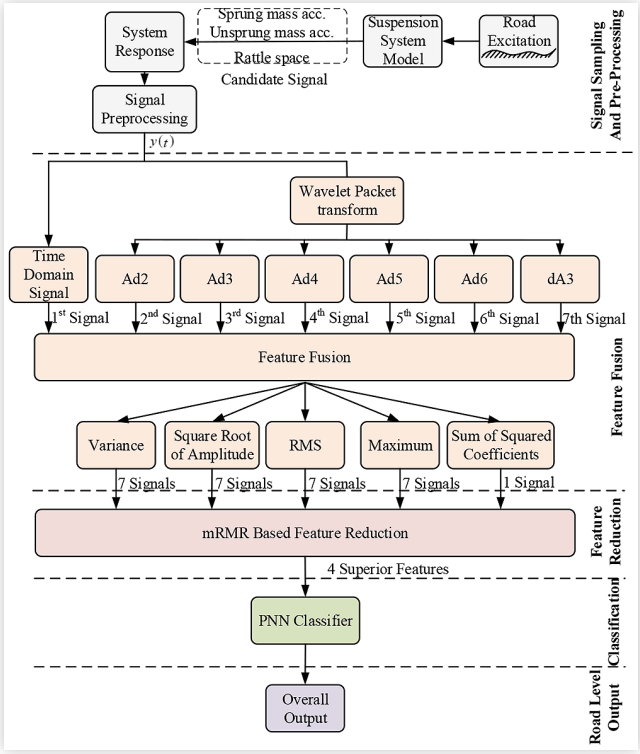

suspension system are sampled and upper frequency bound with rate of 100Hz and 31.3Hz, and the corresponding pre-processing, e.g. low pass filter and windowing, are then performed.

Step 2: Feature Calculation and Fusion. To obtain the features of various frequency ranges, the method of wavelet packet transformation is used to decompose the acquired signals. Seven categories are then generated for selecting the previous 29 features, including the first five approximation components Ad2, Ad3… Ad6, the first detail component dA3 and original signals in the time domain. Some statistics parameters, e.g. variance, root mean square (RMS), maximum, square root of amplitude, sum of squared coefficients, are used to analyzed the seven categories.

Step 3: Feature Reduction. To further solve the dimensionality problem, the minimum redundancy maximum relevance (mRMR) approach is used to select features from the previously obtained 29 features [27]. The mutual information (MI) is used to describe a criterion between the relationship *a* with *b*; the corresponding function is defined:

$$I(a,b)=\sum_{i,j}p(a_i,b_j)\log\frac{p(a_i,b_j)}{p(a_i)\,p(b_j)} \tag{10}$$

Where, $p(a, b)$ represents the probabilistic distribution; $p(a)$ and $p(b)$ represents the marginal probabilities, respectively. Given a signal of length *M* with variables *a* and *b*, the functions of $p(a, b)$, $p(a)$ and $p(b)$ can be calculated using the Gaussian kernel estimator [28]. With the features described in (10), the improved mRMR approach can generate a superior feature set by calculating the all three candidate signals for various features.

FIGURE 6 Flow chart of traditional PNN approach

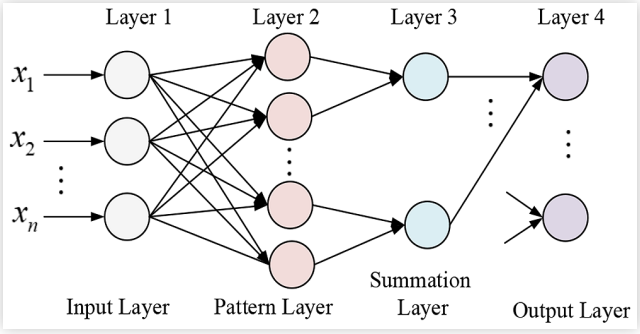

TABLE 3 Values of *Q* and *R* of suspension system under various road input

Road Level	*Q* Value	*R* Value	
		The Acceleration of Sprung mass	The Acceleration of Unsprung mass
ISO-*A*	0.0022	0.0001	0.0015
ISO-*B*	0.0088	0.0004	0.006
ISO-*C*	0.0351	0.0016	0.024
ISO-*D*	0.1406	0.0064	0.096
ISO-*E*	0.5624	0.0256	0.384
ISO-*F*	2.2495	0.1024	1.536
ISO-*G*	8.9979	0.4096	6.144
ISO-*H*	35.992	1.6384	24.576

Step 4: Probabilistic Neural Network (PNN) Classification: A PNN approach is proposed to train the data set and produce a function to compute the features parameters of different categories following the superior feature set generated in Step 3. The structure of traditional PNN is shown in Figure 6. A traditional PNN includes four layers, where the data of analysis system is imported from the input layer into the other layers. The number of neurons within the various layers is equal to the number of patters in the training process.

Remark 1: Numbers of the 4th output layer are equal to numbers of categories, and each neurons of output layer is binary. More details can be found in [26].

Based on the above analysis, the corresponding system process noise covariance ***Q*** and measurement noise covariance ***R*** for suspension system can be calculated as shown in Table 3.

3.2. Representation for AUKF Algorithm

Based on the traditional UKF can be calculated by combing the system state Eq. (9). The expression is given as [29, 30]:

$$\begin{aligned}
&\chi_0 = \overline{x};\ \ \chi_i = \overline{x} + (\sqrt{(n+\lambda)\mathbf{P}})_i; i = 1,2,\cdots n;\\
&\chi_i = \overline{x} - (\sqrt{(n+\lambda)\mathbf{P}})_i; i = 1,2,\cdots n;\\
&\varpi_m^0 = \frac{\lambda}{n+\lambda}; \varpi_c^0 = \frac{\lambda}{n+\lambda} + 1 - \alpha^2 + \beta;\\
&\varpi_m^i = \varpi_c^i = \frac{1}{2}(n+\lambda);\ \ \lambda = \alpha^2(n+\kappa) - p;
\end{aligned} \tag{11}$$

FIGURE 7 Flow chart of AUKF algorithm for semi-active suspension system

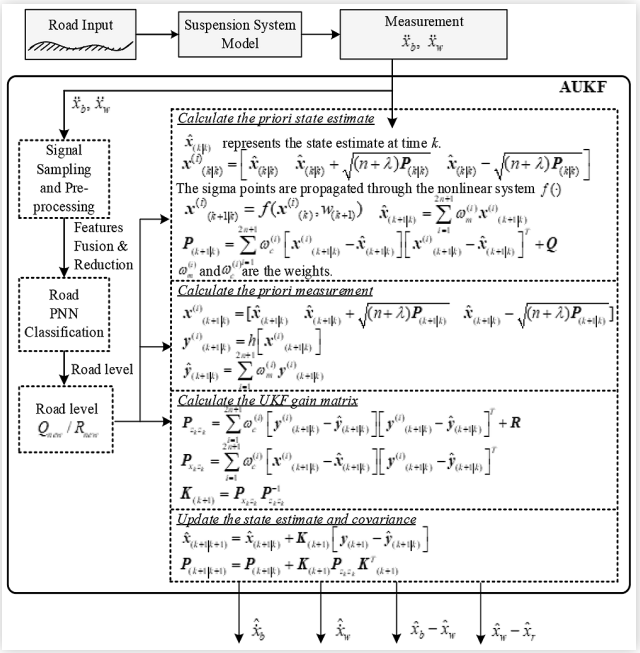

Where, λ represents the scaling parameter, α represents a small positive value, and β is used to include the priori information of state $\mathbf{x}$. $\sqrt{(n+\lambda)\mathbf{P}_x}$ is the ith row of the matrix square root [29].The time-update and filter gain are calculated as follows.

$$\begin{aligned}
&\hat{x}_{k+1}^- = \sum_{i=0}^{2n} \varpi_i^m \chi_{k|k-1};\ \ p_k^- = \sum_{i=0}^{2n} \varpi_m^i (\chi_{i,k|k-1} - \hat{x}_k^-)(\chi_{i,k|k-1} - \hat{x}_k^-)^T + Q_k;\\
&P_{zk} = \sum_{i=0}^{2n} \varpi_c^i \{y_i - \overline{y}\}\{y_i - \overline{y}\}^T + R_k;\ \overline{y} = \sum_{i=0}^{2n} \varpi_m^i y_i;\\
&P_{xkzk} = \sum_{i=0}^{2n} \varpi_c^i (\chi_{i,k|k-1} - \hat{y}_k^-)(\chi_{i,k|k-1} - \hat{y}_k^-)^T;\\
&K_k = P_{xkzk} P_{xkzk}^{-1};\ \ \hat{x}_k = x_k + K_k(y_k - \hat{y}_k^-);\ \ P_k = P_k^- - K_k P_{zk} K_k^T
\end{aligned} \tag{12}$$

where, P_k is the estimation error variance matrix, K_k represents UKF gain. Note that Q and R are adopted as shown in Table 3. Then, the method of road classifier and UKF are proposed to produce the AUKF. Using the process of AUKF algorithm, Q and R need to be matched information about perturbation w_k and v_k in Eq. (9). A flow chart of the proposed AUKF approach is shown in Figure 7, and the higher accuracy of state estimation can be acquired. More details can be defined in [30].

4. Analysis for MPC Algorithm

In this section, an adaptive MPC algorithm based road classification identification is developed to improve the performance of semi-active suspension system. Firstly, the responses

FIGURE 8 Flow chart of the proposed adaptive MPC algorithm

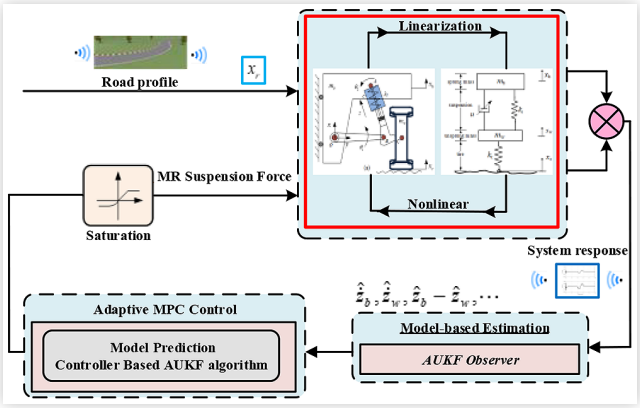

of suspension system are measured. Secondly, using the road classification approach and UKF algorithm, the adaptive UKF strategy is formed to estimate the suspension states. Then, the observer-based MPC algorithm is proposed to improve the suspension performance under the constraint forces of semi-active suspension. The flow chart of the proposed controller is shown in Figure 8. More details can be stated as follows.

Based on the MPC theory, the Eq. (9) can be changed as follows [31].

$$\begin{cases} \Delta x(k+1) = H(k)x(k) + F(k)\Delta u(k) + \Gamma \Delta w(k) \\ y(k) = C(k)\Delta x(k) + D(k)\Delta u(k) + y(k-1) \end{cases} \tag{13}$$

Where, $x(k)$ are the states; $u(k)$ is the control input; $y(k)$ is the output; $w(k)$ are the state noise; $\Delta x(k)=x(k)-x(k-1)$; $\Delta u(k)=u(k)-u(k-1)$; $\Delta w(k)=w(k)-w(k-1)$.

The objective function is employed to calculate both the error of reference tracking and the effort of control algorithm, and the optimal objective can be obtained [30].

$$\min_{u_0,u_1,\ldots,u_{N-1}} J = \min_{u_0,u_1,\ldots,u_{N-1}} \sum_{i=1}^{M-1} \begin{bmatrix} w_{i+1}^{y} \left\| y(k+i+1|k) - y_{ref}(k+i+1|k) \right\|^2 \\ + w_i^{u} \left\| u(k+i+1|k) \right\|^2 \end{bmatrix} \tag{14}$$

s.t.

$$\begin{aligned} y_{min} \le y(k) \le y_{max}, k = 0,1,\ldots N-1 \\ u_{min} \le u(k) \le u_{max}, k = 0,1,\ldots N-1 \end{aligned} \tag{15}$$

Where, N is the predictive length; w^u and w^y are the weights for the control input u and the output y.

The following assumptions should be satisfied when analyzing the MPC approach:

a. Estimation states of $x(k)$ and $y(k)$ should be known under the k step.
b. Control variables are constant under the control domain.
c. Error value of control disturbance are constant under the k+1 step.

Then, the system states and output from the step k to p can be calculated as follows:

$$\begin{aligned} \Delta x(k+1|k) &= H\Delta\hat{x}(k) + F\Delta u(k) + \Gamma\Delta w(k) \\ \Delta x(k+2|k) &= H^2\Delta\hat{x}(k) + HF\Delta u(k) + F\Delta \boldsymbol{u}(k+1) + H\Gamma\Delta w(k) \\ &\vdots \\ \Delta x(k+p|k) &= H^p\Delta\hat{x}(k) + H^{p-1}F\Delta u(k) + H^{p-2}F\Delta u(k+1) \\ &\quad + \cdots + F\Delta u(k+p-1) + H^{p-1}\Gamma\Delta w(k) \end{aligned} \tag{16}$$

$$\begin{aligned} y(k|k) &= y(k) \\ y(k+1|k) &= CH\Delta\hat{x}(k) + CF\Delta u(k) + C\Gamma\Delta w(k) + D\Delta u(k) + y(k) \\ y(k+2|k) &= (CH^2 + CH)\Delta\hat{x}(k) + (CHF + CF)\Delta u(k) \\ &\quad + CF\Delta u(k+1) + (CH\Gamma + C\Gamma)\Delta w(k) + D\Delta u(k) + y(k) \\ y(k+3|k) &= \sum_{i=1}^{3}(CH^i)\Delta\hat{x}(k) + \sum_{i=1}^{3}(CH^{i-1}F)\Delta u(k) + \cdots \\ &\quad + CF\Delta u(k+2) + \sum_{i=1}^{3}(CH^{i-1}\Gamma)\Delta w(k) + D\Delta u(k) + y(k) \\ &\vdots \\ y(k+p|k) &= \sum_{i=1}^{p} CH^i\Delta\hat{x}(k) + \sum_{i=1}^{p} CH^{i-1}F\Delta u(k) + \cdots \\ &\quad + CF\Delta u(k+p-1) + \sum_{i=1}^{p} CH^{i-1}\Gamma\Delta w(k) + D\Delta \boldsymbol{u}(k) + y(k) \end{aligned} \tag{17}$$

Where, p is the predictive step; if m is the control step, the relationship between m and p is $p \ge m$.

Taking Eq. (16) and Eq. (17) into Eq. (14), and the objective function can be rewritten by removing the terms without the control input.

$$\min_{\mathbf{u}} \mathbf{J} = \mathbf{u}^T\left(\mathbf{F}^T\mathbf{Q}\mathbf{F} + \mathbf{R}\right)\mathbf{u} + 2\mathbf{x}^T\mathbf{H}^T\mathbf{Q}\mathbf{F}\mathbf{u} + 2\mathbf{w}^T\Gamma^T\mathbf{Q}\Gamma\mathbf{u} \tag{18}$$

The optimal trajectory can be calculated by using partial differential $J(u)$ under without constraint. The corresponding control force can be rewritten as:

$$\mathbf{u}_{opt} = -\mathbf{u}^T\left(\mathbf{F}^T\mathbf{Q}\mathbf{F} + \mathbf{R}\right)^{-1}\mathbf{F}^T\mathbf{Q}\left(\mathbf{H}\mathbf{x} + \Gamma\mathbf{w}\right) \tag{19}$$

Assuming that the system state are constraint for semi-active suspension:

$$\mathbf{L} \le \mathbf{x} \le \mathbf{U} \tag{20}$$

Eq. (13) can be rewritten as follows.

$$\begin{aligned} \mathrm{L} - \mathrm{F}\hat{u} - \Gamma\hat{w} \le Hx(k) \le \mathrm{u} - \mathrm{F}\hat{u} - \Gamma\hat{w}; \\ \begin{bmatrix} \mathrm{F} \\ -\mathrm{F} \end{bmatrix}\mathrm{u} \le \begin{bmatrix} u \\ -L \end{bmatrix} + \begin{bmatrix} -H & -\Gamma \\ H & \Gamma \end{bmatrix}\begin{bmatrix} x(k) \\ w \end{bmatrix}; \end{aligned} \tag{21}$$

Then, the system is a typical Quadratic Program (QP) problem [32], which can be written as:

$$\begin{aligned} &\min_{u} J = \mathrm{u}^T\left(\mathrm{F}^T Q\mathrm{F} + R\right)\mathrm{u} + 2\mathrm{x}^T\mathrm{H}^T Q\mathrm{F}\mathrm{u} + 2w^T\Gamma^T Q\Gamma\mathrm{u} \\ &s.t. \quad \begin{bmatrix} F \\ -F \end{bmatrix}\mathrm{u} \le \begin{bmatrix} U \\ -L \end{bmatrix} + \begin{bmatrix} -H & -\Gamma \\ H & \Gamma \end{bmatrix}\begin{bmatrix} x(k) \\ w \end{bmatrix}; \end{aligned} \tag{22}$$

The Karush-Kuhn-Tucker condition is given below:

$$\begin{aligned}
&\left(F^T QF + R\right)u + x^T H^T Q\Gamma_u + \begin{bmatrix} F \\ -F \end{bmatrix}^T \lambda = 0 \\
&\begin{bmatrix} F \\ -F \end{bmatrix} u \le \begin{bmatrix} U \\ -L \end{bmatrix} + \begin{bmatrix} -H & -\Gamma \\ H & \Gamma \end{bmatrix} \begin{bmatrix} x(t) \\ w \end{bmatrix} \le 0 \\
&\lambda^T \left(\begin{bmatrix} F \\ -F \end{bmatrix} u \le \begin{bmatrix} U \\ -L \end{bmatrix} + \begin{bmatrix} -H & -\Gamma \\ H & \Gamma \end{bmatrix} \begin{bmatrix} x(t) \\ w \end{bmatrix} \right) = 0 \\
&\lambda \ge 0
\end{aligned} \tag{23}$$

The QP problem can be solved by using the interior point method [33]. More details state in [31, 34].

5. Analysis for Simulation and Validation

In this section, we adopt the observer-based adaptive MPC algorithm scheme derived in Section 4 to optimize the performance of semi-active suspension under various road input.

5.1. Simulation Results of PNN Road Identification

Using the response-based PNN classifier in Section 3, the results of road classification are shown in Figures 9-11. According to the results shown above, the measurable responses of suspension system can observer road classification with a relatively short time interval (1 s). For larger road level variation, e.g. from *B* to *D*, from *F* to *C*, and from *C* to *A*; some local errors (red circle shown) appear and road levels are incorrectly identified to previous excitation levels. In fact, when road level changes, the transitions of suspension system responses are unavoidable and increase or decrease the PSD of system responses and then lead to classification errors [26].

FIGURE 9 Identification results of sprung mass acceleration

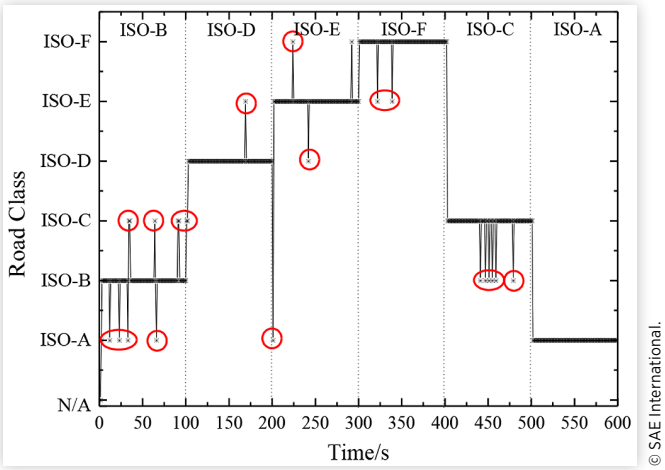

FIGURE 10 Identification results of unsprung mass acceleration

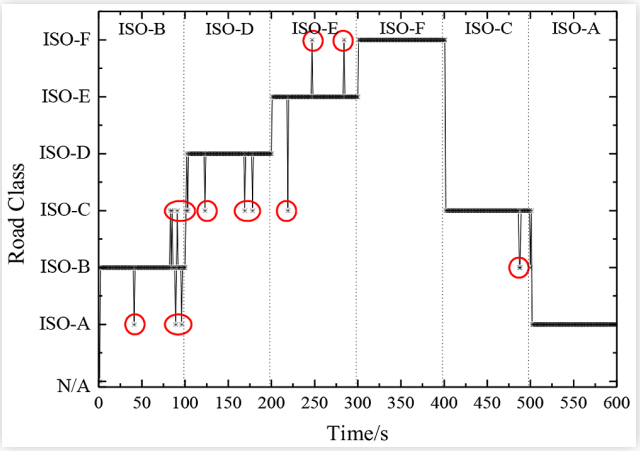

FIGURE 11 Identification results of rattle space

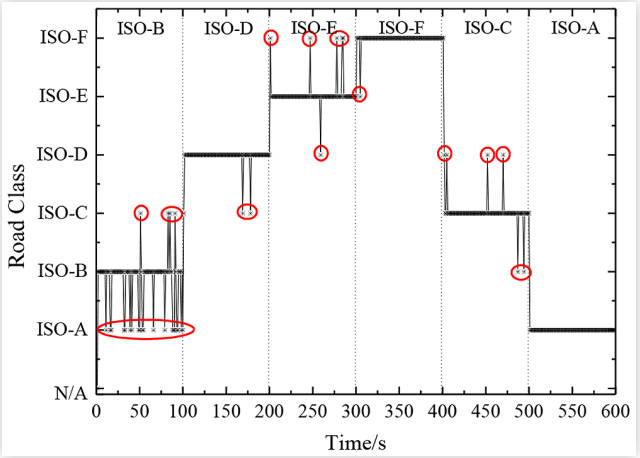

5.2. Adaptive MPC Control Verification

To validate the control performance of MPC algorithm for semi-active suspension, a constrained optimal control (COC) algorithm is used to compare the road handing and ride comfort for semi-active suspension system. More details about COC algorithm can be found in [35, 36].According to the Sections 3and 4 mentioned, the setting parameters of MPC approach can be obtained in Table 4.

Table 5 show that the proposed MPC algorithm compared with COC and passive approaches improves more than 10% for ride comfort and road handing under the ISO-*C* excitation.

To further validate the control performance of MPC approach, the response results of sprung mass acceleration are proposed to compare the COC algorithm and passive approach at 0~1.2 seconds as shown in Figure 12. The corresponding results of tire load force are shown in Figure 13. As for the semi-active predictive controllers, since dampers can only dissipate energy, no action is observed during this period. We can conclude that the differences of different control algorithms generally come from whether road information is used,

TABLE 4 Values of *Q* and *R* of suspension system under various road input

Working Description	Parameters Setting (units)
Velocity of vehicle body	40km/h
Road excitation	ISO-*C*
Constrain of rattle space	120mm
Time step of MPC algorithm	20 step (10 step for training, others for predictive)
Predictive time of MPC algorithm	0.01s

TABLE 5 Calculation RMS values of different modes for semi-active suspension under ISO-*C* road excitation (40km/h)

Control Strategy	RMS values	
	Sprung mass acceleration(m/s^2)	Tire Displacement (m)
Passive	0.866	0.00259
COC	0.791(8.66%↓)	0.00248(4.25%↓)
MPC	0.736(15.1%↓)	0.00245(5.41%↓)

FIGURE 12 Results of comparing ride comfort for semi-active suspension (MPC/COC/Passive situation)

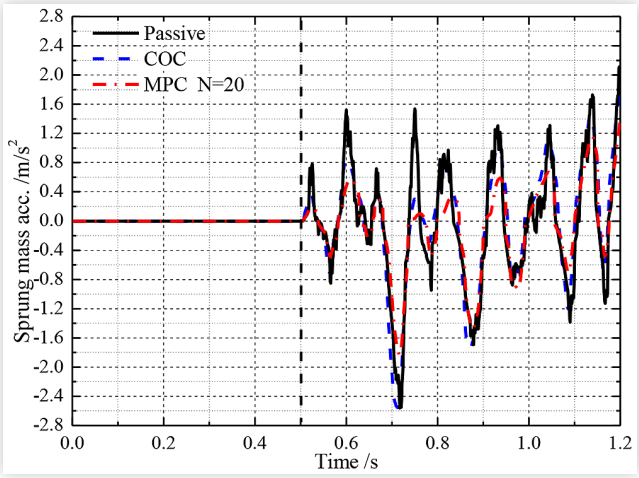

FIGURE 13 Results of comparing road handing for semi-active suspension (MPC/COC/Passive situation)

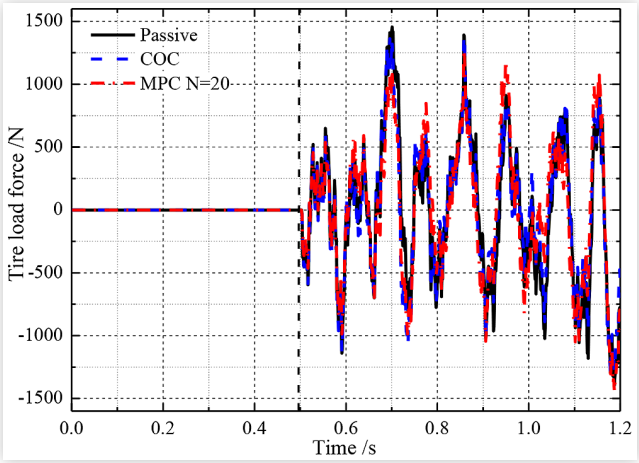

FIGURE 14 Results of MPC algorithm damping force in the time domain

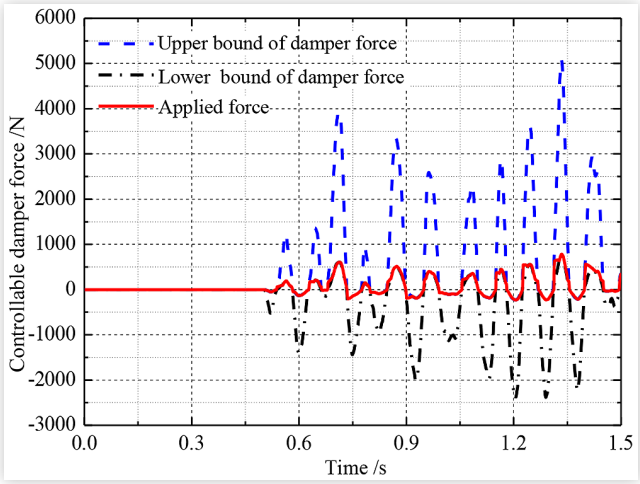

FIGURE 15 Results of COC algorithm damping force in the time domain

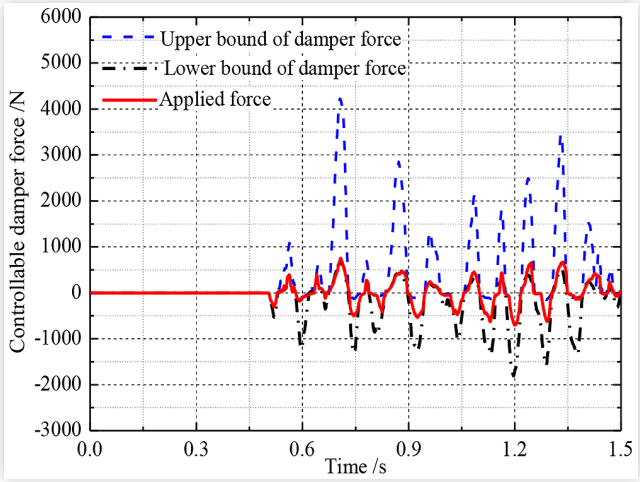

and whether the damping force constraints are considered. We present the damper force and its corresponding bounds in the time domain (0~1.5 seconds) in Figures 14 and 15. Figures 14 and 15 show that the controllable damper forces of COC and MPC algorithms are inside the force bounds. Compared to COC algorithm, the proposed MPC algorithm damper force in Figures 14 and 15 is smaller and occurs at a lower frequency.

Furthermore, by comparing the COC algorithm simulation results, the higher performance of ride comfort and road handing for semi-active suspension can be acquired by using the proposed algorithm.

6. Conclusions

A novel observer-based adaptive MPC algorithm combined with suspension system was developed to optimize the performance of semi-active suspension. Using the mentioned

approaches, the higher accuracy of state observer and better performance of ride comfort and road handing for semi-active suspension system was obtained. The main conclusions are as follows:

1. Based on the semi-active suspension response, the PNN classifier approach was employed to identify the road classification, and it was used to develop the AUKF algorithm. Simulation results show that the proposed approach could obtain a more accurate data.
2. The observer-based adaptive MPC algorithm was compared and validated through the COC algorithm and passive mode. Simulation show that the RMS values of sprung mass acceleration and tire displacement for semi-active suspension system improves more that 10% under the ISO-*C* excitation.

In the future, the proposed method will be applied to the actual road input, and we will mainly focus on experiment validation of adaptive MPC algorithm and its application for nonlinear chassis vehicle controllable system.

References

1. Ahamed, R., Choi, S.B., and Ferdaus, M.M., "A State of Art Magneto-Rheological Materials and Their Potential Aplications," *Journal of Intelligent Materials Systems and Structures*, 2018, doi:10.1177/1045389X18 754350.
2. Tseng, H.E. and Hrovat, D., "State of the Art Survey: Active and Semi-Active Suspension Control," *Vehicle System Dynamics* 53:1034-1063, 2015.
3. Rigatos, G., Siano, P., and Pessolano, S., "Design of Active Suspension Control System with the Use of Kalman Filter-Based Disturbances Estimator," *Cybernetics and Physics* 1:259-275, 2012.
4. Hu, C., Wang, Z.F., Hamid, T.et al., "MME-EKF-Based Path-Tracking Control of Autonomous Vehicles Considering Input Saturation," *IEEE Transactions on Vehicular Technology*, 2019, doi:10.1109/TVT.2019. 2907696.
5. Sun, Y., Li, L., Yan, B.J.et al., "A Hybrid Algorithm Combining EKF and RLS in Synchronous Estimation of Road Grade and VehicleM ass for a Hybrid Electric Bus," *Mechanical Systems and Signal Processing*, 2015, doi:10.1016/j.ymssp.2015.08.015.
6. Qi, Z.Y., Taheri, S., Wang, B.F.et al., "Estimation of the Tyre-Road Maximum Friction Coefficient and Slip Slope Based on a Novel Tyre Model," *Vehicle System Dynamics* 53:506-525, 2015.
7. Wang, Z.F., Qin, Y.C., Gu, L.et al., "Vehicle System State Estimation Based on Adaptive Unscented Kalman Filtering Combing with Road Classification," *IEEE Access*, 2017, doi:10.1109/ACCESS.2017.2771204.
8. Ren, H.B., Chen, S.Z., Zhao, Y.Z.et al., "State Observer-Based Sliding Mode Control for Semi-Active Hydro-Pneumatic Suspension," *Vehicle System Dynamics* 54:168-190, 2016, doi:10.1080/00423114.2015. 1122818.
9. Hong, S., Lee, C., Borrelli, F.et al., "A Novel Approach for Vehicle Inertial Parameter Identification Using a Dual Kalman Filter," *IEEE Transactions on Intelligent Transportation Systems* 16:151-161, 2015.
10. Huang, X. and Wang, J., "Real-Time Estimation of Center of Gravity Position for Lightweight Vehicles Using Combined AKF-EKF Method," *IEEE Transactions on Vehicular Technology* 63:4221-4231, 2014.
11. Soheib, F. and Dugard, L., "An LPV/H∞ integrated vehicle dynamic controller," *IEEE Transaction on Vehicular Technology* 65:1880-1889, 2016.
12. Zhaojian, L., "Developments in Estimation and Control for Cloud-Enabled Automotive Vehicles," Ph.D. thesis, Mechanical Engineering Department, University of Michigan, Michigan, 2016.
13. Sun, X.Q., Yuan, C.C., Cai, Y.F.et al., "Model Predictive Control of an Air Suspension System with Damping Multi-Mode Switching Damper Based on Hybrid Model," *Mechanical Systems and Signal Processing* 90:94-110, 2017, doi:10.1016/j.ymssp. 2017.02.033.
14. Li, H., Yu, J., Chris, H.et al., "Adaptive Sliding-Mode Control for Nonlinear Active Suspension Vehicle Systems Using T-S Fuzzy Approach," *IEEE Transaction on Industrial Electronics* 60:3328-3338, 2013.
15. ISO8601, "Mechanical Vibration-Road Surface Profiles-Reporting of Measured Data," 2016.
16. Wang, Z.F., Dong, M.M., Qin, Y.C.et al., "Suspension System State Estimation Using Adaptive Kalman Filtering Based on Road Classification," *Vehicle System Dynamics* 55:371-398, 2016.
17. Wu, Z.C., Chen, S.Z., and Yang, L., "Model of Road Roughness in Time Domain Based on Rational Function," *Beijing Institute of Technology* 29:795-798, 2009.
18. Wang, Z.F., Dong, M.M., Gu, L.et al., "Influence of Road Excitation and Steering Wheel Input on Vehicle System Dynamic Responses," *Applied Sciences-Basel* 7:570, 2017, doi:10.3390/app7060570.
19. Chiang, H.H. and Lee, L.W., "Optimized Virtual Model Reference Control for Ride and Handling Performance-Oriented Semi-Active Suspension Systems," *IEEE Transaction on Vehicular Technology* 64:1679-1689, 2015.
20. Qin, Y.C., Zhao, F., Wang, Z.F.et al., "Road Comprehensive Analysis for Influence of Controllable Damper Time Delay on Semi-Active Suspension Control Strategies," *Journal of Vibration and Acoustics* 139:371-398, 2017, doi:10.1115/1.4035700.
21. Sun, W.C., Zhao, Z., and Gao, H.J., "Saturated Adaptive Robust Control for Active Suspension Systems," *IEEE Transactions on Industrial Electronics* 60:389-3896, 2013.
22. Na, J., Huang, Y., Wu, X.et al., "Active Adaptive Estimation and Control for Vehicle Suspensions with Prescribed Performance," *IEEE Transactions on Control Systems Technology* 7:1-15, 2017.
23. Savaresi, S.M., Poussot-Vassal, and Spelta, C., *Semi-Active Suspension Control Design for Vehicles* (MA: Elsevier, 2010).
24. Qin, Y.C., Dong, M.M., Zhao, F.et al., "Road Profile Classification for Vehicle Semi-Active Suspension System Based on Adaptive Neuro-Fuzzy Inference System," in *Proceedings of the 54rd IEEE Conference on Decision and Control*, 2015, Vol. 1, 1538-1543.

25. Cheng, C.Z. and Cebon, D., "Parameter and State Estimation for Articulated Heavy Vehicles," *Vehicle System Dynamics* 49:399-418, 2011.
26. Qin, Y.C., Xiang, C.L., Wang, Z.F.et al., "Road Excitation Classification for Semi-Active Suspension System Based on System Response," *Journal of Vibration and Control*, 2017, doi:0.1177/1077546317693432.
27. Peng, H., Long, F., and Ding, C., "Feature Selection Based on Mutual Information Criteria of Max-Dependency, Max-Relevance, and Min-Redundancy," *IEEE Transactions on Pattern Analysis and Machine Intelligence* 27:1226-1238, 2005.
28. Cai, Y., Huang, T., Hu, L.et al., "Prediction of Lysine Ubiquitination with mRMR Feature Selection and Analysis," *Amino Acids* 42:1387-1395, 2012.
29. Zhao, Y., Liang, B., Iwnicki, S.et al., "Friction Coefficient Estimation Using an Unscented Kalman Filter," *Vehicle System Dynamics* 52:220-234, 2014.
30. Wang, Z.F., Qin, Y.C., Gu, L.et al., "Vehicle System State Estimation Based on Adaptive Unscented Kalman Filtering Combing with Road Classification," *IEEE Access*, 2017, doi:10.1109/ACCESS.2017.2771204.
31. Huang, Y.J., Wang, H., Khajepour, A.et al., "Model Predictive Control Power Management Strategies for HEVs: A Review," *Journal of Power Sources* 341:91-106, 2017.
32. Borrelli, F., Bemporad, A., and Morari, M., *Predictive Control for Linear and Hybrid Systems* (Berlin: Springer, 2014), 6-196.
33. Jin, Z.L., Li, J.X., Huang, Y.J.et al., "Study on Rollover Index and Stability for a Triaxle Bus," *Chinese Journal of Mechanical Enginerring* 32:1-15, 2019.
34. Pacejia, H.B., *Tire and Vehicle Dynamics* (Oxford, U.K.: Butterworth-Heinemann, 2002), 5-240.
35. Qin, Y.C., Wang, Z.F., Yuan, K.et al., "Comprehensive Analysis and Optimization of Dynamic Vibration Absorbing Structures for Electric Vehicles Driven by In-Wheel Motors," *Automotive Innovation* 2:254-262, 2019.
36. Sergio, M.S., Charles, P.V., Cristiano, S.et al., *Semi-Active Suspension Control Design for Vehicles* (MA: Elsevier, 2010), 10-120.

Contact Information

Zhenfeng Wang
CATARC (Tianjin) Automotive Engineering Research Institute Co., Ltd
China Automotive Technology and Research Center Co., Ltd.
68 East Xianfeng Road, Dongli District, Tianjin, 300300, P. R. China

Acknowledgments

This work was supported of China Automotive Technology and Research Centre Co., Ltd. (Grant No. 19201203 and Grant No. 19210111).

ISSN 0148-7191